ATA Memo #26

RFI Survey at the RPA

G. R. Harp and R. F. Ackermann
April 30, 2001

Abstract

A survey of the accessible sky at the Rapid Prototype Array (RPA) was made using single-dish measurements. We present full sky maps over the available frequency range. Some interesting features include: 1) physical features blocking the antennas' view are clearly seen, such as the hillside and barn, 2) virtually all the man-made radio sources appear to have right hand circular polarization, 3) at any time there may be dozens of satellites in view, even with the limited coverage at the RPA, and 4) the very large primary beam of the RPA antennas make them susceptible to polarization distortion at the beam edges. These measurements also provide calibrations for the difference in cable length to each feed of a given antenna.

Experiment

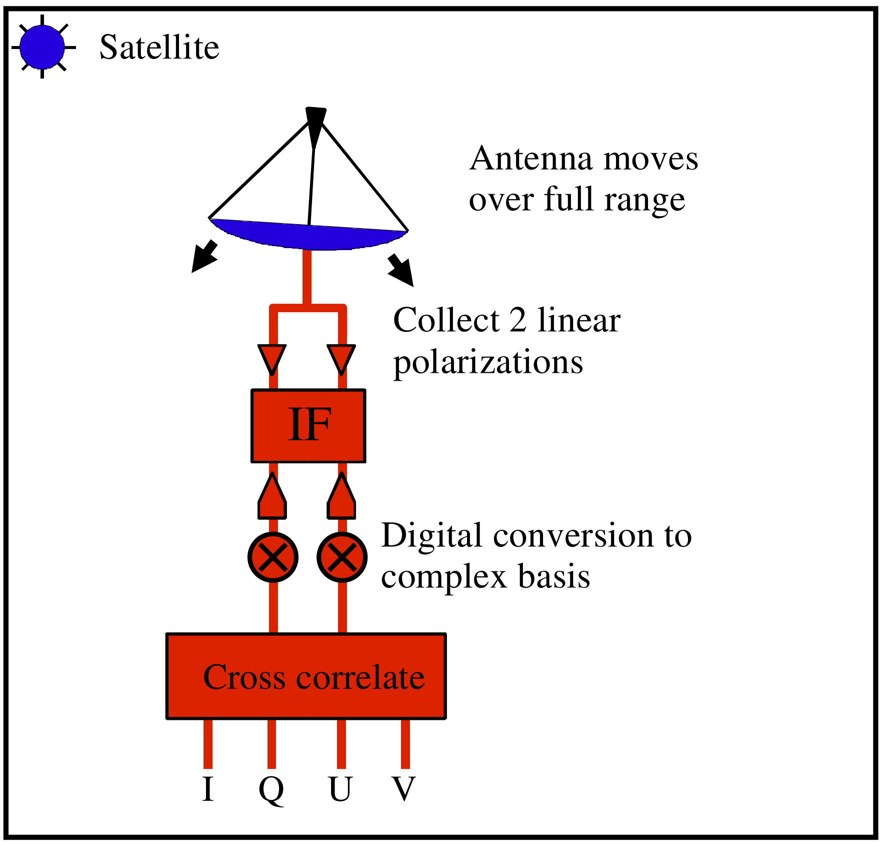

Fig. 1. Summary of data collection technique.

All the results presented here are single-dish measurements. The antenna is swept over a grid of points in the horizontal (x) and vertical (y) where $-\pi/2 < x, y < \pi/2$ in steps of 0.015 radians. This provides a coordinate system where the radius is linear in elevation angle, though the image is circumferentially stretched at large radii. The step size is to be compared with the primary beam diameter whose FWHM is ~0.06 radians. In this way, data were acquired over the full range of motion of the antenna drives, while (x, y) points that lie outside of this range were skipped.

Throughout the measurements, all seven antennas were moved together and images were acquired from all antenna. Only a few highly-reduced images from RPA7 are presented here. We plan to publish a complete set of "raw" frequency dependent images on the ATA software website at http://kitimar.seti.org/intranet/ata/software.

At each (x, y) point, the antenna pauses and acquires data. Data are taken in 10 MHz frequency steps (the nominal IF bandpass) centered on integer multiples of 10 MHz. At each frequency 128,000 samples (~4 ms) of the IF output are acquired in two polarizations. The sampling rate is 30 MHz (Nyquist = 15MHz) with the nominal IF bandpass covering the range 2.5-12.5 MHz. The IF bandpass filter does not have perfectly sharp edges, and the IF signal falls –20 dB over 2 MHz on either side of the nominal bandpass. Thus there is some overlap between the data we acquire in successive frequency steps, and a strong feature near e.g. 1555 MHz might appear in both the 1550 and 1560 MHz frequency bins.

The nominal RF bandwidth is 1400-1630 MHz, though the cutoff on either side is about 20 MHz wide. Accordingly, 23-27 maps can be obtained using a 10 MHz step size. Extra maps were sometimes obtained at higher and lower frequencies to further test the electronics.

At each frequency interval, f, samples were acquired from both linear feeds (X and Y) on each antenna, and zero-lag Stokes parameters were formed from the sampled data according to

$$I(f) = \int (\tilde{E}_x \cdot \tilde{E}_x^* + \tilde{E}_y \cdot \tilde{E}_y^*)\, dt\,, \tag{1}$$

$$Q(f) = \int (\tilde{E}_x \cdot \tilde{E}_x^* - \tilde{E}_y \cdot \tilde{E}_y^*)\, dt\,, \tag{2}$$

$$U(f) = 2\,\mathrm{Re}\left(\int \tilde{E}_x \cdot \tilde{E}_y^*\, dt\right), \text{ and} \tag{3}$$

$$V(f) = 2\,\mathrm{Im}\left(\int \tilde{E}_x \cdot \tilde{E}_y^*\, dt\right). \tag{4}$$

Recall that the Stokes parameters all have units of power. The first, I, is simply the total power coming in both feeds. Q and U are measures of the linearly polarized components of the radiation, whereas V measures the circularly polarized component.

Q, U, and V may all be positive or negative, with the sign indicating the sense of the polarization. Specifically, V is positive for RHCP and negative for LHCP.

In the present context we are also interested in a few parameters that can be derived from the Stokes parameters. The polarized (P) and unpolarized (N) components of the radiation are given by

$$P(f) = \sqrt{Q^2 + U^2 + V^2}, \quad \text{and} \tag{5}$$

$$N(f) = I(f) - P(f), \tag{6}$$

while the linearly polarized component (L) is

$$L(f) = \sqrt{Q^2 + U^2}. \tag{7}$$

Calibrating the Cable Lengths

On each antenna, the cables coming from the X and Y feeds differ by a length Δl. As we show below, this difference is typically of order 20 cm and is small compared to the correlation length, ξ, for a 10 MHz bandwidth ($\xi = c/\Delta f =$ 30 m). As a result, we need not worry about correlation loss between the signals coming from the two feeds. However, Δl also introduces a phase shift,

$$\Delta\phi = 2\pi\, \Delta l / \lambda, \tag{8}$$

between the X and Y signals. As seen in (1)-(4), the phase shift has no effect on I and Q, but mixes the signal between U and V. To unmix these signals, we apply a simple transformation *after* the fact

$$U' = U \cos\Delta\phi - V \sin\Delta\phi, \tag{9}$$

$$V' = U \sin\Delta\phi + V \cos\Delta\phi. \tag{10}$$

In general $\Delta\phi$ is frequency dependent, and a different value is used at each frequency step. Because $\Delta l \ll \xi$, it is sufficient to use the same $\Delta\phi$ throughout a single frequency interval. This provides a great simplification, since otherwise it would not be possible to unmix the U and V signals after formation of the Stokes parameters.

The transformation (9)-(10) requires knowledge of Δl, which we determine by observing satellites with known polarization characteristics. For example, Solidaridad F2 (1533 MHz) and Iridium (1626 MHz) are both known to transmit RHCP radiation. By observing one satellite, we can determine Δl up to an integral number of wavelengths, N. The second satellite provides N.

Using this method Δl was determined for each antenna. However, preliminary examination of the resulting sky maps showed that all of the observed satellites at the RPA had a dominant circular polarization. This fact was then used to further refine Δl by minimizing $U'(f)$ at all frequencies (see eqs. (9)-(10)). In all cases, the refinement procedure changed Δl by no more than 1 cm. The estimated error in our determination of Δl is 0.5 cm. The values of Δl for each antenna are shown in figure 2.

Antenna	RPA1	RPA2	RPA3	RPA4	RPA5	RPA6	RPA7
Δl (m)	-0.081	0.186	-0.021	3.270	-0.234	0.296	-0.048

Fig. 2. The cable length difference, Δl, between the two polarizations on each RPA antenna, as determined from satellite polarization data.

RPA4 presents an interesting anomaly. Here Δl is 10 times higher than on any other antenna. A discussion with Geoff Bower revealed that one of the cables on RPA4 had been damaged and was replaced by a different cable, which was about 3 m longer than the original. This provides an excellent verification of our methods.

Total Power

Figure 3 shows a map of $I(f)$ over the entire accessible sky as measured with RPA7. This map took approximately 2.5 days to acquire. To enhance the visibility of weaker features in the image, we plot $I_p = \sqrt{I_m}$, where I_m is the measured intensity. (I_p is the electric field amplitude.) The data at each frequency step are plotted on a monochromatic scale whose hue is related to frequency as indicated by the color bar. Twenty five false color images are then superimposed to form figure 3.

Here the angular projection has zenith at image center and the horizon is indicated by the white circle. The linear relationship between elevation angle and pixel position is indicated by the scale at the bottom. The north-south axis runs vertically in the figure, with north at the top and east on the left. All the sky maps presented below were analyzed in the same way, unless specified otherwise.

There are many features to understand in figure 3. Features with intense color have a narrow bandwidth, hence are man-made. Features that appear almost gray in color are broadband, and have nearly the same intensity at all frequencies. For example, the white blob in the lower left hand corner is a region where the telescope points toward the hillside. The broadband features all have a slightly reddish tinge because the telescope gain decreases slightly as a function of frequency.

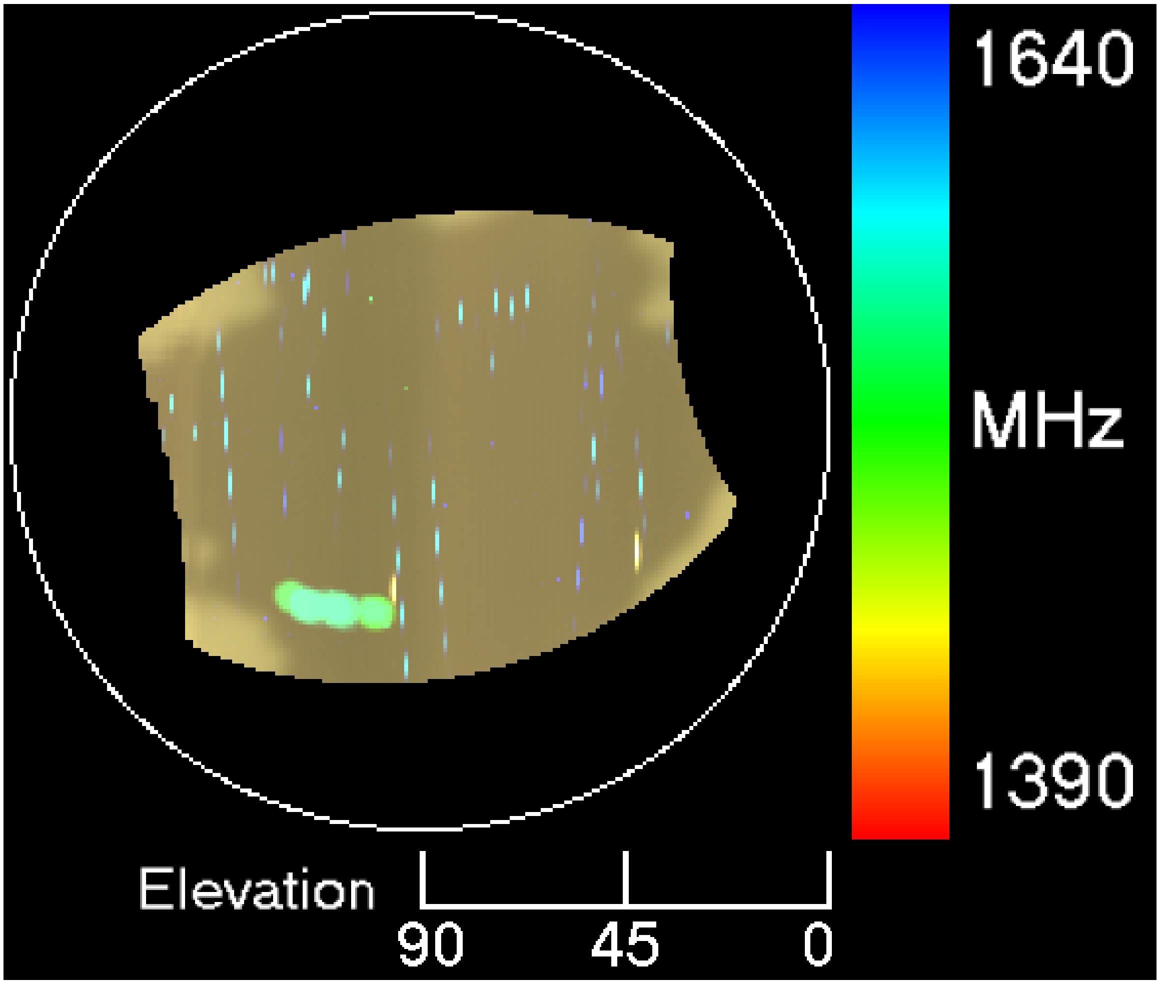

Fig. 3. Total power, $I(f)$, as measured from RPA7.

There are three types of features associated with satellites (or aircraft). The circular shapes on the lower left are satellites in the geosynchronous belt. These features stay put long enough to be fully measured, and their shape is indicative of the primary beam. The narrow stripes running from north to south are moving satellites. These satellites move slowly on the time scale of a single scan line, but quickly on the time scale of the entire map. Such satellites intersect the primary beam in one scan line, but disappear before the antenna returns for the next scan line. Hence, the streaks are as long as the primary beam width, but only one scan line wide. There are also a few point-like features. These could be fast moving LEO's, satellites that infrequently pulse their power output, or possibly aircraft.

Unpolarized Radiation

The polarization sensitivity of the RPA offers an opportunity to decompose figure 3 into its natural and man-made components. The unpolarized component ($N(f)$) of figure 3 is plotted in figure 4.

Here we have artificially enhanced the contrast in the image relative to figure 3. Note that the image is almost monochromatic, because most unpolarized sources are broadband. (The color features are obviously artifacts related to the brightest satellites. Because the noise signal scales as the square root of the total power, and some of the noise is uncorrelated between the two polarizations, the brightest satellites can generate these features.)

There are two bright noise like linear features indicated by arrows in the figure. These are the sun, which passed through the telescope's view twice during the measurement. Around the circumference of the image, five blobs appear. These are: at 12 o'clock a stand of trees, at 2 o'clock the telephone pole, at 4 o'clock the barn, at 7 o'clock the hillside, and at 10 o'clock the welder's shed.

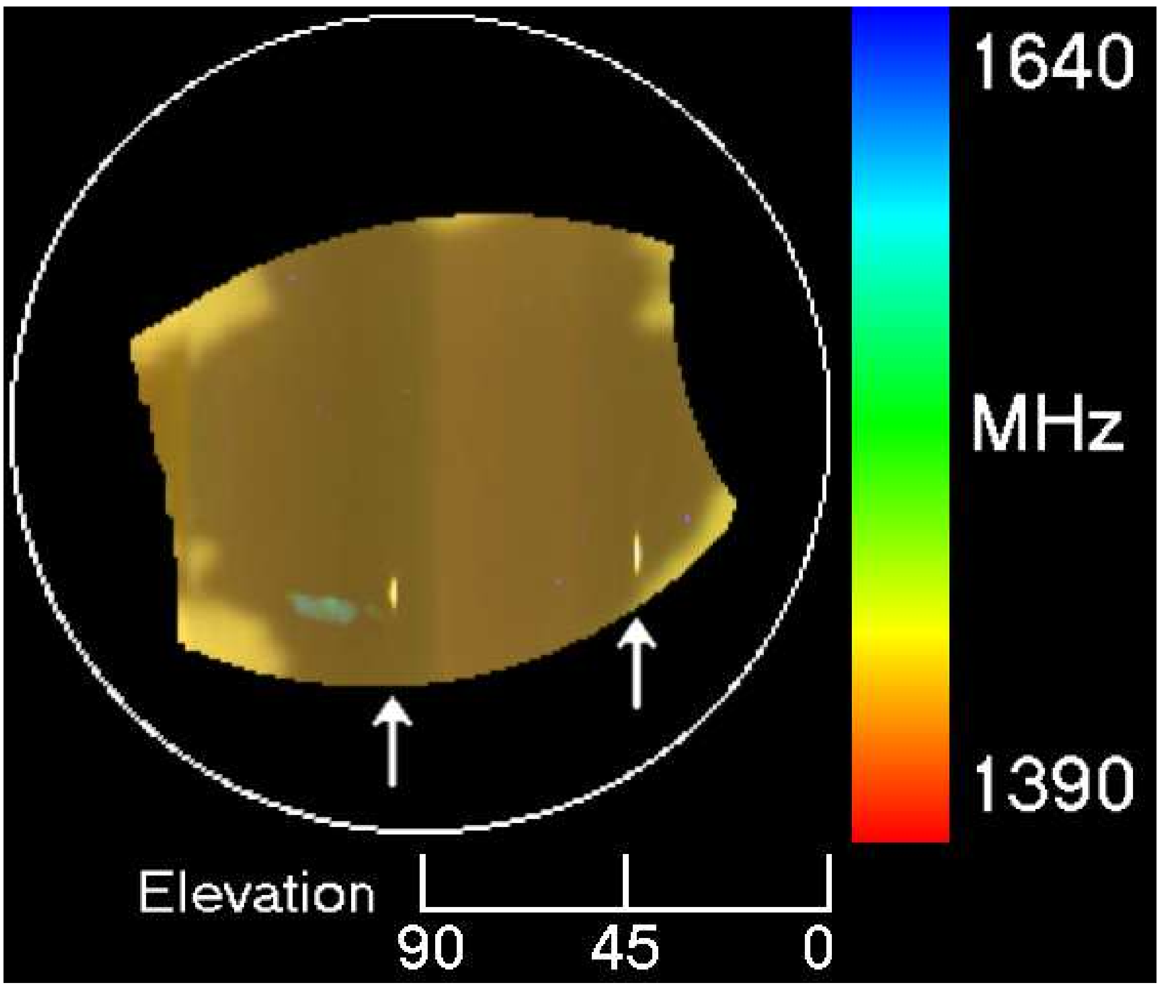

Fig. 4. The unpolarized component of fig. 3.

Circular Polarization

Figure 5 displays the circularly polarized intensity ($|V(f)|$) from figure 3. All the narrow band sources were found to have a predominant circular polarization. This is easily understood, since the ionosphere would introduce a Faraday rotation into linearly polarized signals from satellites, hence the satellite builders always choose to transmit circularly polarized light. Note that circular polarization makes an excellent discriminator against natural radio sources, as none of the broadband features of figure 4 appear in figure 5.

Notice that there are no red features in figure 3. This is because the frequency range in the vicinity of 1420 MHz is protected for radio astronomy applications. Indeed, we observe no polarized features for any frequency below 1520 MHz (green in figure 5).

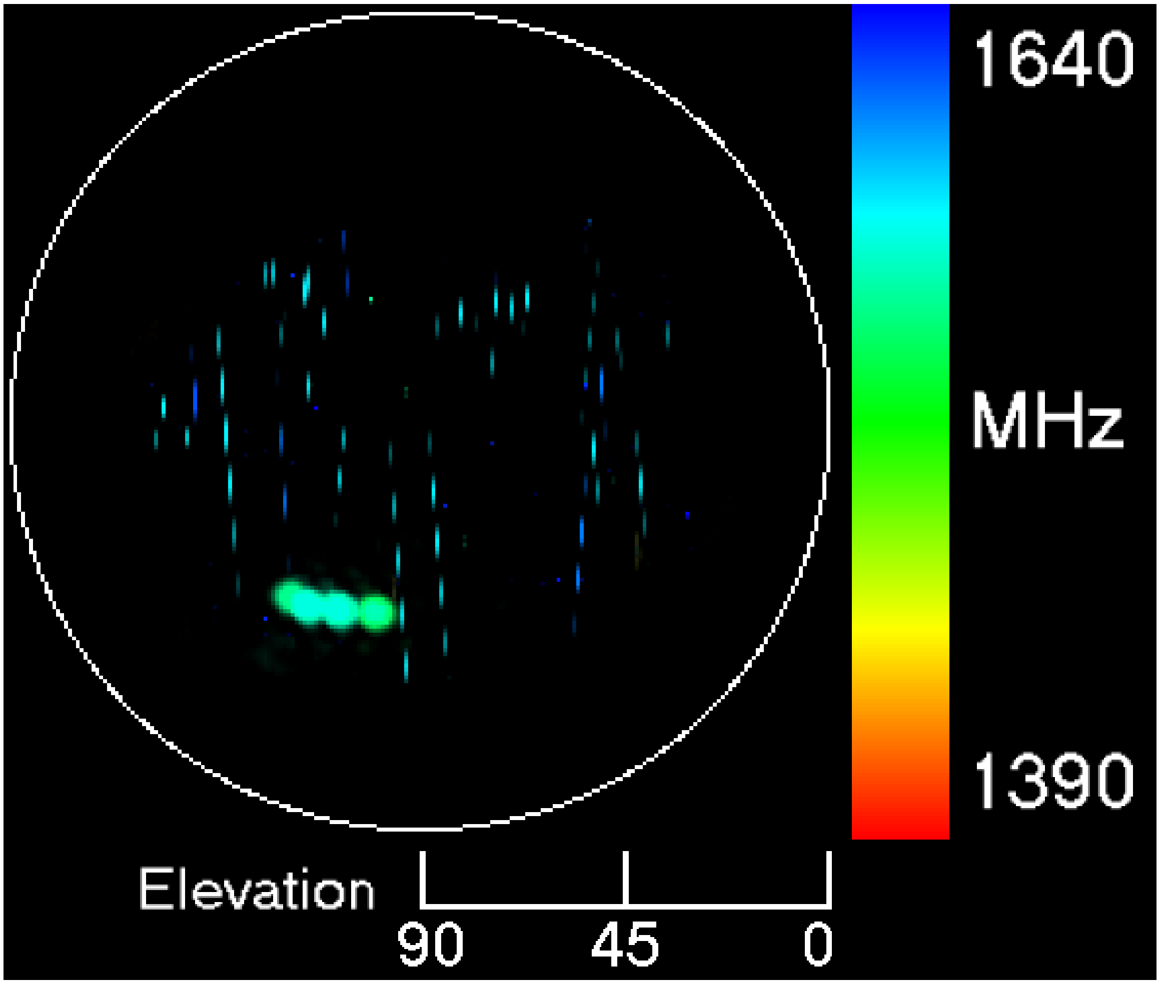

Fig. 5. Circularly polarized component of figure 3.

The satellites in figure 5 can be identified both by their positions and their frequencies. The geostationary satellites (blue-green ovals) include Solidaridad F1 and F2 which transmit in the vicinity of 1540 MHz. The light blue stripes are GPS, which show up in the 1580 MHz frequency slice. Note that the GPS satellites move slowly enough that they can appear in multiple scan lines. Because this image was acquired with north-south scan lines rastered from right to left, we see that most of the GPS satellites were caught as they traversed from south to north.

The deep blue stripes are probably Iridium, as these features appear most strongly in the 1620 MHz frequency slice. The dark blue points occur at 1640 MHz. This is above the expected frequency range for the Iridium pager pulse. (Indeed, they are slightly above the nominal RF bandpass. However, an examination of the bandpass shows there is still significant sensitivity at the frequency.) We have not identified these features (nor the green points), but they are probably fast moving LEO's which remain in the primary beam for the duration of only one pixel. Some of these points are quite intense however, and indicate a very strong unidentified radio source which deserves further study.

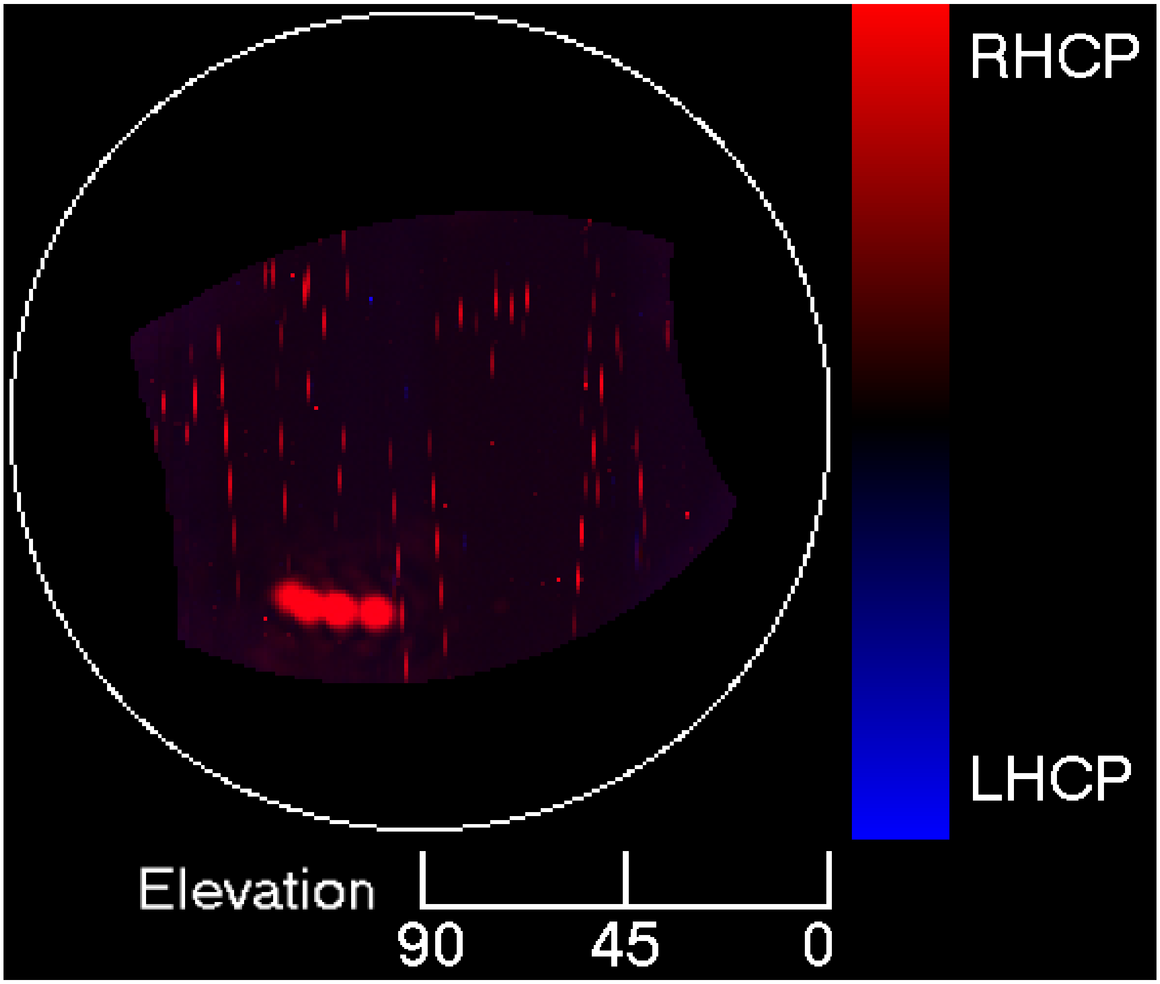

Fig. 6. The data from figure 5 are replotted, this time using a color scale that distinguishes RHCP from LHCP radiation.

The Stokes parameter $V(f)$ allows us to distinguish RHCP from LHCP radiation according to its sign (positive and negative, respectively). This is done in figure 6, where the frequency-integrated intensity of $V(f)$ is displayed. Here the color scale is used to distinguish RHCP (red) from LCHP radiation (blue). We see that virtually all the satellites transmit RHCP radiation. There seems to be no particular reason for this, except perhaps convention among the satellite makers.

Linear Polarization and Polarization Purity

As mentioned above, all the man-made radiation we measure has a predominant circular polarization. In our measurements, the linearly polarized component is at least 7 times smaller than the circularly polarized component everywhere in the image. A contrast enhanced display of $|L(f)|$ is depicted in figure 7. This figure closely reflects figure 5, with the notable difference that there is fine structure present in the images of the geostationary satellites. Close inspection reveals that this fine structure is also present in some of the GPS and Iridium stripes.

Because satellites are point sources, this fine structure must be an artifact of the measurement device. It turns out that the RPA antennas do not have constant polarization sensitivity over their entire primary beam. This is easily understood by examining their physical structure. The four metal tubes that support the feed tend to scatter linearly polarized radiation that is aligned with their axis. Let us choose a coordinate system where the x-axis is aligned with one set of support tubes, while the y-axis is aligned with the other set.

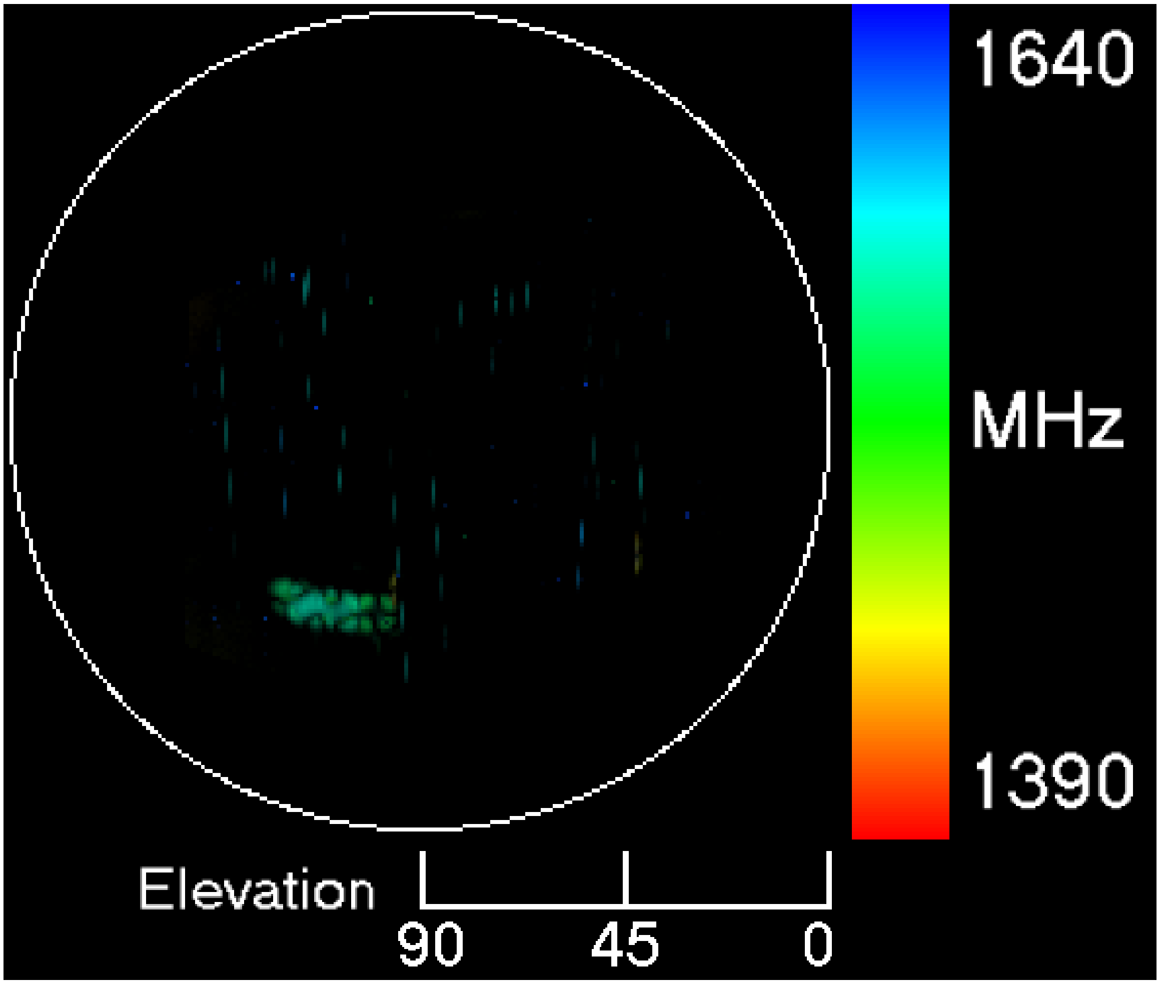

Fig. 7. Contrast enhanced display of the linearly polarized component of the radiation.

When the dish is aimed directly at a satellite, symmetry requires that the x- and y-polarized radiation is scattered in equal amounts, hence circular polarization is preserved. However, if the dish points to one side of the satellite, even when the satellite remains in the primary beam, then the symmetry is broken. Generally one polarization (either x or y) will be preferentially scattered, introducing a net linear polarization into the measurement. To support this analysis, we present in figure 8 a contrast enhanced plot of $U(f)$ where, as in figure 6, positive values of $U(f)$ are displayed in red while negative values are blue. To further simplify the display, we show only the 1540 MHz frequency slice.

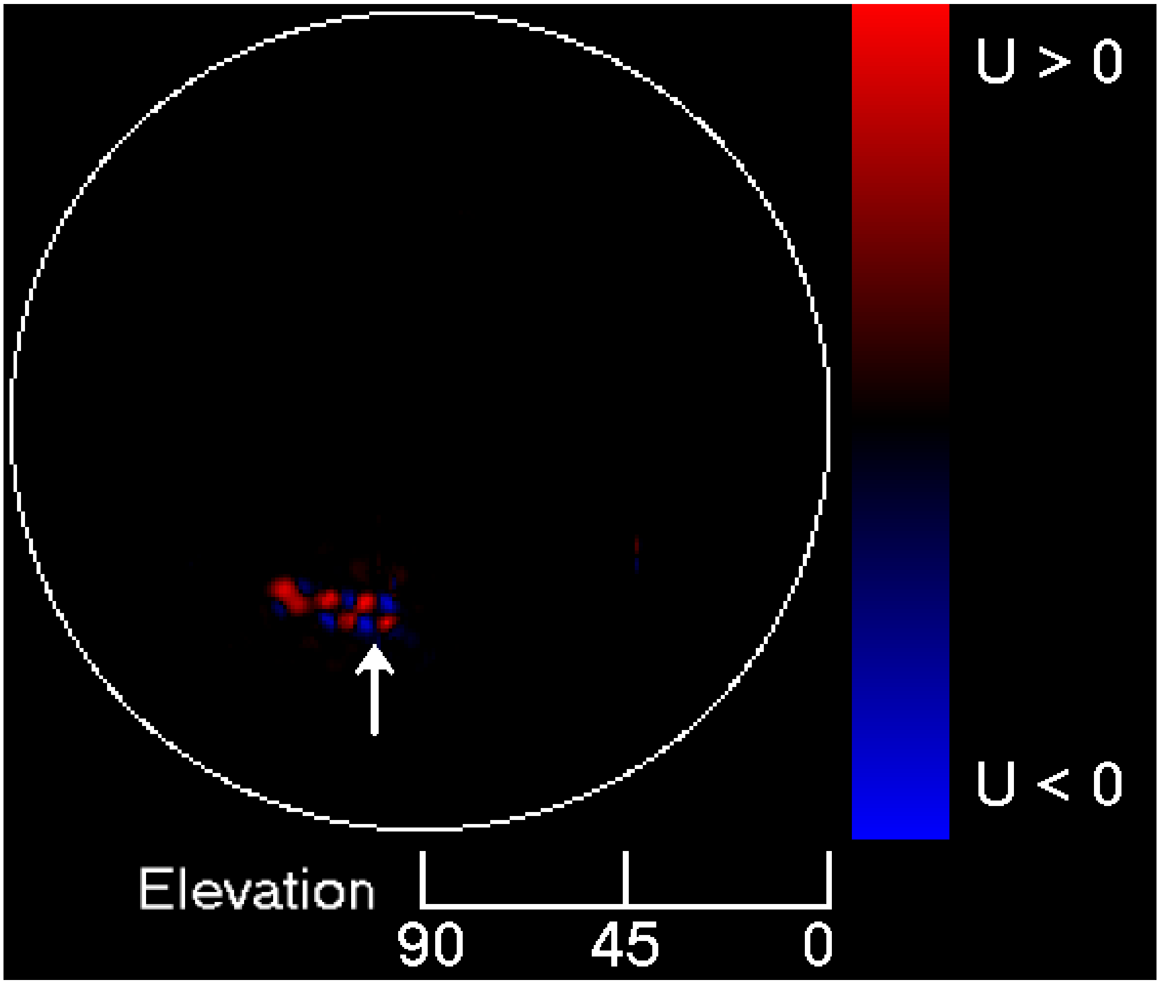

Fig. 8. Display of the 1540 MHz frequency slice of the linearly polarized radiation.

There are three quadrupole-like structures visible in figure 8, one of which is identified by the white arrow. The black center of the indicated structure is the position of Solidaridad F2. The black center indicates that when the antenna is pointed directly at the satellite, then the measured radiation is purely circular. However, when the antenna pointing is displaced in a direction of 45 degrees relative to this center (parallel to one of the feed legs) then a linear polarization is introduced into the measurement, which we arbitrarily call "X" polarized. If the antenna displacement is at –45 degrees, then the sense of the linear polarization is reversed, i.e. it becomes "Y" polarized.

We note that such polarization distortion is evident only because the primary beam is so large. If we were using a much larger dish, then we could make measurements of the satellite only for small angular displacements from bore sight. In this case, the distortion (which varies quadratically with displacement) would be greatly reduced. Hence we have discovered yet another way in which the performance of small dishes is qualitatively different from that of large dishes.

Theoretical Sky Map

Because the radiation properties of most satellites are well characterized, we can model this radiation and compare it with our experiments. This is done in figure 9. Here the map labeled Experiment is the frequency-integrated power taken from figure 3 on a false color scale. The color bar at right is linear in power, and notice that we have suppressed display of background noise by setting a threshold (5%) below which the intensity is plotted as black. The power scale is arbitrary, and chosen such that the geostationary satellites have approximately the same power value in experiment as they do in theory.

The map labeled Theory is courtesy David DeBoer, shows a calculation of the expected sky flux at the front-end of an RPA antenna assuming matched polarization (RHC) from published radiated powers. The "streaked" signals have been generated to resemble the measured data and show just the power present in the scan that would intersect near bore sight from Iridium and GPS. For Iridium, the power level was set by assuming values ranging from the ringer tone to modest traffic.

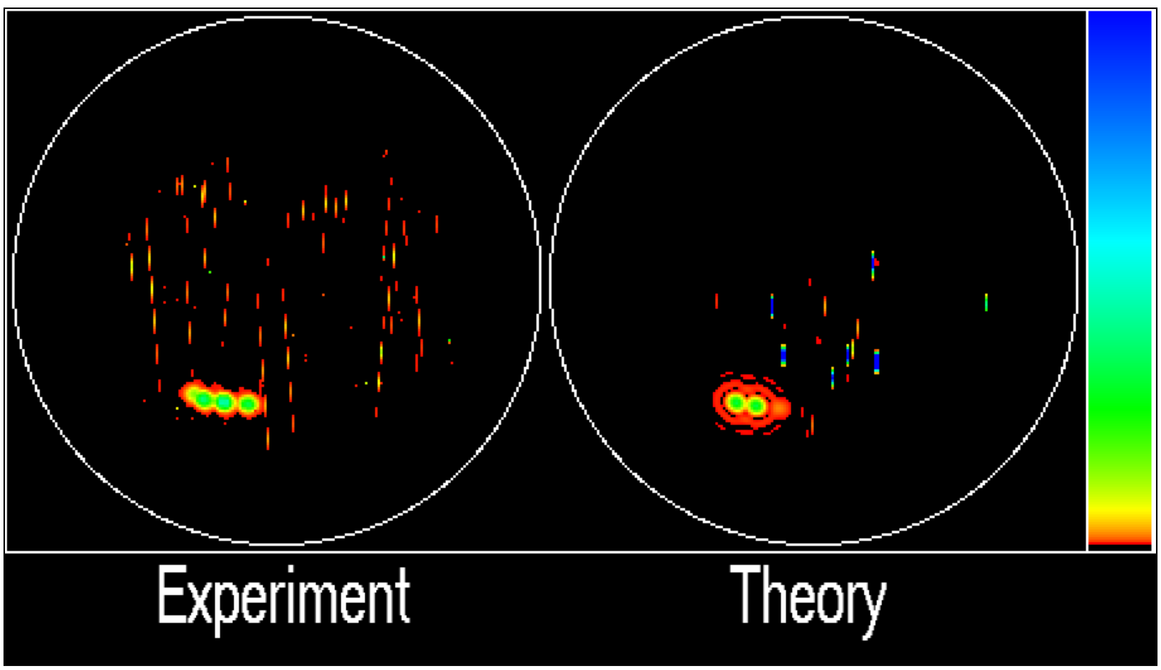

Fig. 9. Comparison of frequency-integrated circularly polarized radiation (Experiment) with a model sky map generated from published power values (Theory). The color bar maps to a linear power scale with a peak power of 0.0013 mW for the Theory map. The Experiment scale is also linear, but its peak value is arbitrary.

There are a couple points of interest. In the experimental map, there are four geostationary satellites while in the theoretical map there are only three. This demonstrates the importance of using actual RFI measurements in characterizing the fluid situation of satellite communications. Secondly, the experimental measurements of Iridium never have quite as high power as those predicted by theory. This might be because of the frequency dependence of the experimental gain, which we have not corrected for. Clearly, future experiments should perform this correction.

Conclusions

What conclusions can we draw from this data that relate to the ATA? First we note that there is no specific time scale associated with man-made signals. We have observed signals that vary with time scales of minutes, hours, or not at all. Another point is that these maps can be loosely interpreted as a kind of snapshot of the sky at the RPA. From this we conclude that there are dozens of satellites in the sky at any one time. With the much wider bandwidth of the ATA, this number might approach 100! This should be kept in mind in the consideration of RFI excision techniques.

Finally, the wide primary beam of the ATA antennas might make the ATA susceptible to polarization distortion toward the edges of the primary beam. Note that the ATA antenna has a clear aperture and should be much less susceptible to polarization distortion than the RPA's prime focus design. However, the broken symmetry of the ATA Gregorian design will likely favor one linear polarization over the other, especially when the antenna is pointed "above" the source in the vertical plane.

It seems likely that when performing narrow-field polarization maps (as with a correlator), the ATA will have comparable if not better polarization uniformity than other telescopes employing larger dishes. However, if one attempts to utilize the entire ATA primary beam for polarization dependent measurements, the polarization sensitivity will have to be carefully calibrated.